Flexible and Printed Electronics

TOPICAL REVIEW

Recent advances in modeling organic electrochemical transistors

Renan Colucci[1], Henrique Frulani de Paula Barbosa[1,2], Florian Günther[1], Priscila Cavassin[1] and Gregório Couto Faria[1] (ORCID)

[1] Instituto de Física de São Carlos, Universidade de São Paulo, CP 369, 13660-970, São Carlos, SP, Brazil
[2] Departamento de Engenharia de Materiais, Escola de Engenharia de São Carlos, Universidade de São Paulo, 13563-120, São Carlos, SP, Brazil

E-mail: gcfaria@ifsc.usp.br

Abstract

Organic electrochemical transistors (OECTs) have been successfully used as transducers in applications requiring the conversion of ion fluxes to electronic current. These applications range from regular biosensors to sophisticated devices for neuron recording and stimulation. For the rational optimization and understanding of the fundamentals of OECTs and OECT-based applications, however, it is essential to develop in-depth theoretical predictions of experimental data. Here, we review seminal works on modeling both the steady state and transient behavior of OECTs and discuss their strengths and weaknesses. Given that OECTs have been used and applied by a diverse community with very different backgrounds, our intention is to clarify and to extend most of the theoretical developments established so far. Special attention is given to the early models, while trying to make them accessible for everyone in the field of organic bioelectronics.

1. Introduction

While biological systems, such as living cells, communicate through ionic fluxes, man-made technologies are mainly based on electronic fluxes [1, 2]. Thus, in order to effectively interface and mimic biological systems, it is essential to produce devices that are able to transduce, and therefore, support both electronic and ionic current efficiently [2–4]. In fact, there is a large number of materials with such an ability, which are known in the literature as mixed ionic-electronic conductors [5, 6].

Among others, ceramics and semiconducting polymers are the two main classes of mixed conductors that have been extensively studied in the recent years [5–7]. While ceramics normally conduct ions better than electrons, conjugated polymers tend to show a more balanced ratio between ionic and electronic conductivities [5]. Besides, mixed conducting polymer devices tend to operate in the sub-unit voltage regime, being compatible with both aqueous and biological media [2, 8]. Moreover, polymers permit the fabrication of flexible and foldable structures [8–11] and their ink-based processing characteristics allow for cheaper and easier to manufacture devices [8,

12–14]. Out of the many available platforms that transduce ion-to-electron fluxes, the organic electrochemical transistor (OECT) has been the focus of attention, especially in the field of bioelectronics. This is mainly due to its great success in a wide range of applications, including alcohol sensors [15], virus detection [16], health care monitoring systems [17–19], impedance biosensors [20, 21], neural recording and stimulation [22], and neuromorphic computing [3, 23, 24], to name a few.

In order to keep up with the increasing number of valuable and creative applications, rational material and device optimizations must be targeted proportionally. This, however, requires an in-depth understanding of the device working mechanisms, which encompasses the development of theoretical modeling of experimental data. In fact, there is a large number of proposed models that partially or fully describe both the steady and transient behavior of OECTs [25–37]. Nevertheless, the rich nature of mixed ionic-electronic conductivity in disordered conjugated polymers is far from been completely understood and is still a hot and exciting topic of research [2, 8, 38, 39]. Here, we seek to compile, discuss, and eventually to extend several seminal

Figure 1. (a) Schematic of an OECT and (b) working mechanism of an accumulation mode OECT.
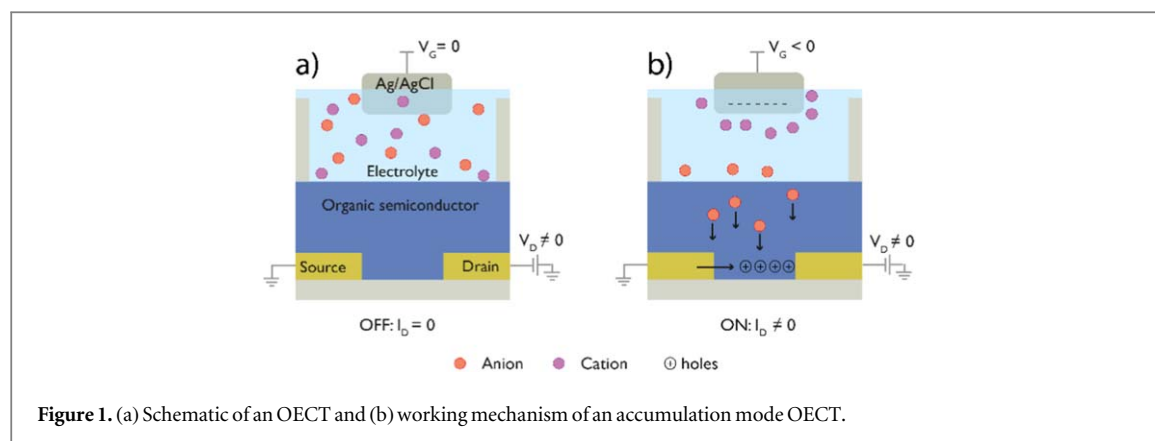
manuscripts on modeling OECT devices [27–29, 31–36]. Given the great number of amazing contributions to the topic, it is virtually impossible to gather and review every single OECT model that has been proposed to date [25–37]. Therefore, we decided to review key models that have been successfully used to describe either the steady state or transient drain current of OECTs. The main part of this review is separated into four main complementary types of models: the Bernards–Malliaras (B-M)-based models (section 3), equivalent circuit models (section 4), and recent developments on a hybrid B-M model and elaborated circuit models (section 5). To complete this review, we are lastly reviewing works that originate from including a diffusion term to the current equation (section 6).

This review was written keeping in mind that organic bioelectronics is a very multidisciplinary research field with professionals and researchers with diverse backgrounds. Therefore, in every possible way, we have tried to fully clarify the models' theoretical derivations and developments. Any mathematical step not given in the main manuscript is thoroughly detailed in the supplementary material available online at stacks. iop.org/FPE/5/013001/mmedia (except for the drift-diffusion models that require computational methods). We hope that this review becomes useful to the bioelectronics community and stimulates further developments in the device physics of OECTs and organic mixed-conductor platforms alike.

2. Principles of OECT operation

The principles of OECT operation have been widely described in the literature and will only be briefly reviewed here. The OECT is a three-terminal device that consists of two pre-patterned electrodes, the source and drain, connected through a semiconducting polymer, defining the transistor channel. The organic active layer is in contact with an electrolyte, where a third electrode (gate) is immersed, as shown in figure 1(a). During operation, the application of a gate voltage induces a charge injection from the electrolyte into the channel, which can either dope or de-dope the semiconducting polymer, leading to a change in the

source-drain current [32, 40] as illustrated in figure 1(b).

OECTs can operate either in the depletion mode or in the accumulation mode. In the former case, the OECT is naturally in its on state (i.e. the active material in the channel is initially doped) and is turned off upon application of a gate voltage (de-doping of the channel). In the latter one, the device is normally off (i.e., initially the semiconducting polymer is in its neutral stage). Upon gate voltage application, ions are introduced from the electrolyte into the polymer film. There, charges are balanced by injection of electronic charges from the source electrode, such that the charge density in the semiconducting polymer, and consequently, its conductivity is increased (figure 1(b)). In a typical p-type accumulation mode transistor, the electrochemical process can be expressed by the following relation:

$$P^0 + Q^- \leftrightarrow P^+Q^- + e^-,$$
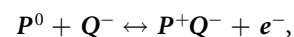
where P is the active polymer, Q is the anion species, and e^- is an electron [23]; n-type doping follows a similar electrochemical reaction, mediated by cations instead of anions. In order to maintain bulk neutrality, for every monovalent ion that enters the active polymer film, an electronic charge must be injected by the electrodes, generating a one-to-one ionic-electronic transducer.

The electrical characteristics of OECTs follow those of traditional transistors. Output and transfer curves are the regular steady-state electrical characterization [8, 41], while pulsed gate voltage and impedance measurements are among the techniques of choice for characterizing the drain-source transient response [35, 40]. In the next sections, we review theoretical models that describe both the steady state and transient working mechanism of OECTs.

3. B-M-based models

One of the first attempts to model both the steady state and transient behavior of OECTs was proposed by Bernards and Malliaras in early 2007 [32]. The model was based on coupling an electronic circuit with an

ionic one, mainly to generate an expression that describes the steady state and transient responses of OECTs (output/transfer and pulsed characteristics). The original model assumes a few simplifications, such a constant charge carrier mobility, which were corrected in follow-up articles [34].

In this section, we start by fully describing the original model by Bernards and Malliaras, explaining the analytical developments and highlighting the steps that could be further improved. The section will also discuss later papers where the B-M model was recalculated incorporating refinements on both mobility and charge density dependency.

3.1. Original B-M model

The original model proposed by Bernards and Malliaras describes both the steady state and transient response of OECTs [32]. Their theoretical developments are independent of each other, and will therefore be treated separately here.

3.1.1. Steady-state behavior

The steady-state current is defined as the operational mode of the transistor where the ionic current, which comes from the electrolyte upon a gate voltage, remains unchanged. In other words, the channel has completely been charged with ions and doping or de-doping of the semiconducting material no longer takes place.

The description of the steady state originates from Ohm's law:

$$J(x) = \sigma E = q\mu\rho(x)\frac{dV(x)}{dx}. \tag{1}$$

Here, the B-M model assumes that the charge carrier mobility μ is constant. This is not particularly true for conjugated polymers, since the mobility may depend on the charge concentration ρ, electric field E, and even temperature Θ [34, 42–45]. Follow-up manuscripts have incorporated a nonuniform mobility [34] and will be discussed later in this review.

In equation (1), J is the current density, σ is the conductivity, q is the elementary charge, and V is the electric potential, the spatial derivative of which defines the electric field. Note that the model assumes the electronic conductivity to be purely one dimensional. This is certainly acceptable for the assumptions made by the model, especially since a constant charge carrier mobility is considered. It is, however, worth mentioning that the ionic uptake is not uniform throughout the bulk of the polymer film. When considering the dependency of the mobility on the charge concentration, a pure one-dimensional description might not be very accurate, and a profile of the ionic uptake through the thickness of the active layer must be assumed and introduced into the model. Recently, such an attempt has been reported in a drift-diffusion based model [29], which is discussed in section 6.

In the B-M model, the electronic conduction is correlated with the ionic flux, by proposing the following expression for the charge carrier density:

$$\rho = \rho_0\left(1 - \frac{Q}{q\rho_0\nu}\right). \tag{2}$$

Here, ρ_0 is the initial charge density of the polymer, Q is the total charge of the ions that penetrates the polymer film upon application a gate voltage, and ν is the volume of the transistor channel. When cations are injected into the channel Q is positive, whereas for injection of anions it is negative. Note that equation (2) applies only to depletion-mode OECTs; i.e., when $Q = 0$ or, equally, $V_g = 0$, $\rho = \rho_0$ and the material is conductive; on the other hand, when $Q = q\rho_0\nu$, $\rho = 0$ the polymer is fully de-doped.

In 2007, the interest in depletion-mode-only models was due to the great success of PEDOT:PSS as active layer in OECT devices. PEDOT:PSS is a polymer blend, where the PEDOT (poly(3,4-ethylenedioxythiophene)) acts as a polycation and PSS, (poly(styrenesulfonate)) as a polyanion. In the mixture, PEDOT becomes highly doped with positive charges (holes), to compensate the sulfonated groups (SO_3^-) on the PSS. Consequently, a PEDOT:PSS-based OECT operates in the depletion mode, since the film is initially conductive and turns off upon the application of gate voltage. In early 2007, the great majority of OECTs were PEDOT:PSS-based devices, and therefore, it made sense to have a depletion-mode-only description of the current-voltage characteristics [46, 47]. Today, however, more and more accumulation mode materials for OECTs are being introduced in the literature [23, 48–52], such that it has become essential to extend the B-M model for this type of operation as well. For instance, the side chain that comprises hydrophilic groups has been successfully incorporated in thiophene-based polymers, yielding water-soluble, neutral polymer films that operate in an accumulation mode [48]. Besides that, a new OECT platform has been recently introduced, enabling virtually all water-insoluble conjugated polymers as possible candidates for the active layer in OECTs [23]. Given that most of the conjugated polymers synthesized to date are neutral in their pristine form, they generate OECTs operating in the accumulation mode. Therefore, an extension of the B-M model to reproduce accumulation mode OECTs is very much desired.

Thus, here we propose an extension of the formulas to describe accumulation mode OECTs. In such a mode of operation, the only difference in the equations discussed so far would be in equation (2). For the accumulation mode, the charge carrier density in the polymer must be proportional to the number of injected ions in the organic film. With that, equation (2) takes the form of [41]
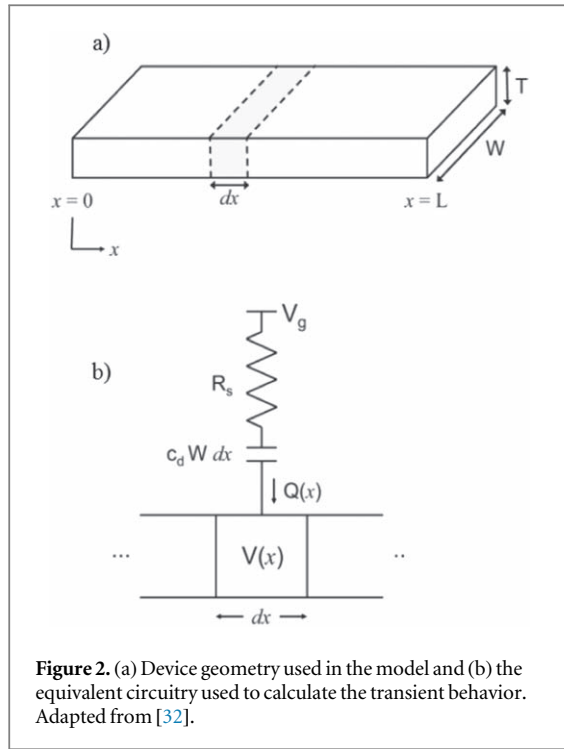
Figure 2. (a) Device geometry used in the model and (b) the equivalent circuitry used to calculate the transient behavior. Adapted from [32].

$$\rho = \left(\frac{Q}{q\nu}\right), \tag{3}$$

where Q, q, and ν are the same physical quantities defined in equation (2). Here we assume that the initial charge concentration ρ_0 of the undoped organic semiconductor is negligible.

In order to calculate the total charge Q of ions injected upon a gate voltage V_g, which enters equations (2) and (3) equally, the model considers the channel to be an ideal capacitor with capacitance C_d. With that said, Q is given by

$$Q(x) = C_d\Delta V = C^*WTdx[V_g - V(x)], \tag{4}$$

where C^* is the capacitance of the film per unit of volume, W is the channel width, T is the film thickness, ΔV is the voltage drop in the transistor channel, and dx is a differential slice in the source-drain direction, see figure 2(a). Despite the B-M model using a capacitance per unit of area, in this review, we will express our formulas in terms of the volumetric capacitance of the channel C^*. This approach is more up to date with the OECT literature, since ions are uptaked throughout the channel volume [6, 38]. In fact, the term μC^* is considered to be the merit factor for an OECT, since C^* accounts for the ionic characteristics and μ for the electronic transport [6].

Also, the B-M model does not account for a possible threshold voltage V_{th}. In fact, a PEDOT:PSS-based OECT has practically zero V_{th} and therefore, it was not be necessary to account for that in the original paper. As new materials [48–52] and platforms [23] are introduced for fabricating organic electrochemical devices, it becomes important to incorporate such a physical quantity in the model. In field-effect transistors (FETs), the threshold voltage is normally associated

with the filling of deep trap states in the semiconductor, before free mobile charges are able to conduct [41]. In electrochemical transistors, such a quantity can be correlated to the onset potential in which the electrochemical reaction can occur (oxidation or reduction potential). Therefore, when accounting for V_{th}, equation (4) becomes:

$$Q(x) = C^*WTdx[V_g - V_{th} - V(x)]. \tag{5}$$

Combining equations (2) and (3) for the depletion or accumulation mode, respectively, with equations (1) and (5), it is possible to obtain the governing equation for the steady-state OECT operation. For the depletion mode, this equation takes the form

$$J = q\mu\rho_0\left[1 - \frac{\{C^*WTdx(V_g - V_{th} - V(x))\}}{q\rho_0 dxWT}\right]$$
$$\times \frac{dV(x)}{dx}$$
$$= q\mu\rho_0\left[1 - \frac{\{C^*(V_g - V_{th} - V(x))\}}{q\rho_0}\right]\frac{dV(x)}{dx}, \tag{6}$$

whereas for accumulation mode OECTs the expression is

$$J = q\mu\frac{\{C^*WTdx\}(V_g - V_{th} - V(x))}{qdxWT}\frac{dV(x)}{dx}$$
$$= \mu C^*(V_g - V_{th} - V(x))\frac{dV(x)}{dx}. \tag{7}$$

Note that in the steady-state response, the current is constant, and therefore, $J = J(x)$. Introducing a pinch-off voltage as being

$$V_p = \frac{q\rho_0}{C^*}, \tag{8}$$

the final expression for the depletion mode (equation (6)) can be simplified to

$$J = q\mu\rho_0\left[1 - \frac{(V_g - V_{th} - V(x))}{V_p}\right]\frac{dV(x)}{dx}. \tag{9}$$

This equation can be readily integrated over the length of the transistor channel. For details on the integration process, refer to the supplementary material. The final analytical expression for the depletion-mode OECT is

$$I = \frac{q\mu\rho_0 WT}{L}\left(1 - \frac{(V_g - V_{th} - V_d/2)}{V_p}\right)V_d, \tag{10}$$

where I is the source-drain current and L is the channel length. For the accumulation mode, the integration of equation (7) yields

$$I = \frac{WT\mu C^*}{L}(V_g - V_{th} - V_d/2)V_d. \tag{11}$$

Note that these expressions do not entirely describe the output characteristics of an OECT, mainly due to their square dependency on V_d. After the saturation current, equations (10) and (11) do not lead
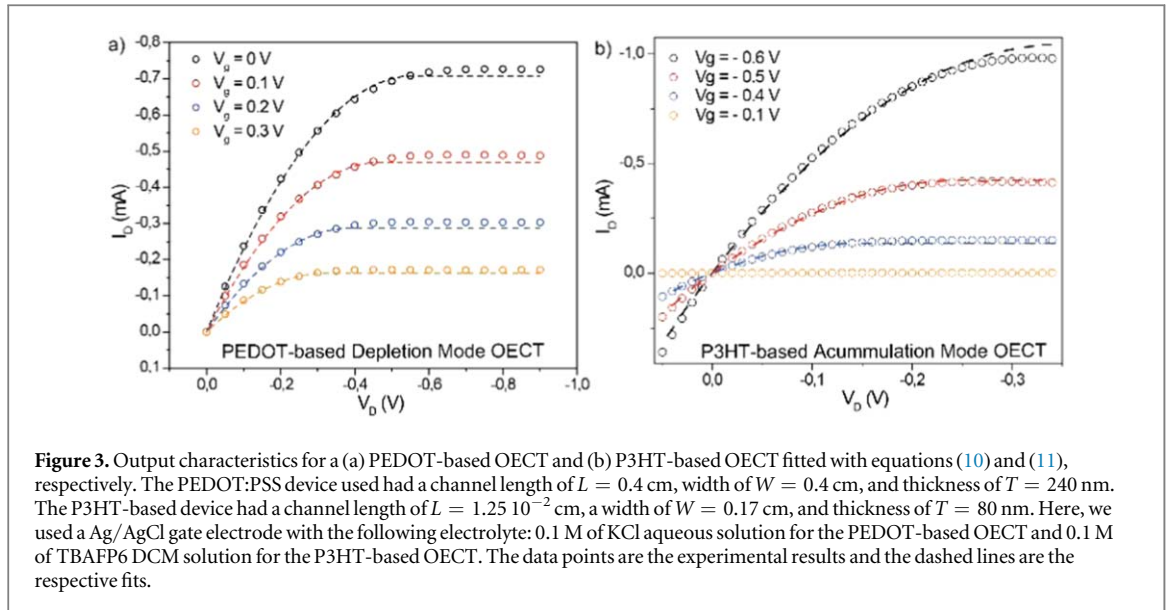
Figure 3. Output characteristics for a (a) PEDOT-based OECT and (b) P3HT-based OECT fitted with equations (10) and (11), respectively. The PEDOT:PSS device used had a channel length of $L = 0.4$ cm, width of $W = 0.4$ cm, and thickness of $T = 240$ nm. The P3HT-based device had a channel length of $L = 1.25 \, 10^{-2}$ cm, a width of $W = 0.17$ cm, and thickness of $T = 80$ nm. Here, we used a Ag/AgCl gate electrode with the following electrolyte: 0.1 M of KCl aqueous solution for the PEDOT-based OECT and 0.1 M of TBAFP6 DCM solution for the P3HT-based OECT. The data points are the experimental results and the dashed lines are the respective fits.

to a constant current. Therefore, the aforementioned equations are only valid until the saturation voltage V_d^{sat}, which can be assigned to the vertexes of the parabolas of equations (10) and (11).

We have used these expressions to fit the experimental results of both the PEDOT:PSS depletion mode and the P3HT accumulation mode OECTs. For the latter we used the liquid-liquid phase separated structure proposed in [23]. Details on the device fabrication and structure can be found in the caption of figure 3. In figure 3(a), equation (10) was used to describe the output characteristic of a regular depletion-mode PEDOT:PSS-based OECT, whereas equation (11) was used to fit the data in figure 3(b), measured from an accumulation mode P3HT-based OECT. A good agreement between the experimental data and the theoretical prediction was achieved for both devices.

The fit formula equation (10) provides two parameters: the pinch-off voltage (equation (8)) and the material conductance $G = \frac{q\mu\rho_0 WT}{L}$. From our measurements shown in figure 3(a), the fit yielded $G \sim 2.2$ mS and $V_p \sim 0.6$ V. The resulting figure of merit μC^*, which can be derived from the ratio $\frac{G}{V_p} = \frac{WT}{L}\mu C^*$, was found to be ~ 150 Fcm^{-1}V^{-1}s^{-1}. This number is in agreement with the literature [6, 39, 53], although it ranges in the highest side of the reported values. For the accumulation mode OECTs, the model directly provides the product between the charge carrier mobility μ and the volumetric capacitance C^*. Fitting the data in figure 3(b) produced an average μC^* of 120 Fcm^{-1}V^{-1}s^{-1} which is also in accordance with the values in the literature reported for P3HT [23].

Finally, the B-M model can be used to model the steady-state response of OECTs biosensors, especially for analyte-based biosensors [54, 55]. Here, the gate potential is corrected by adding an offset voltage, generating an effective gate voltage. Such an offset would
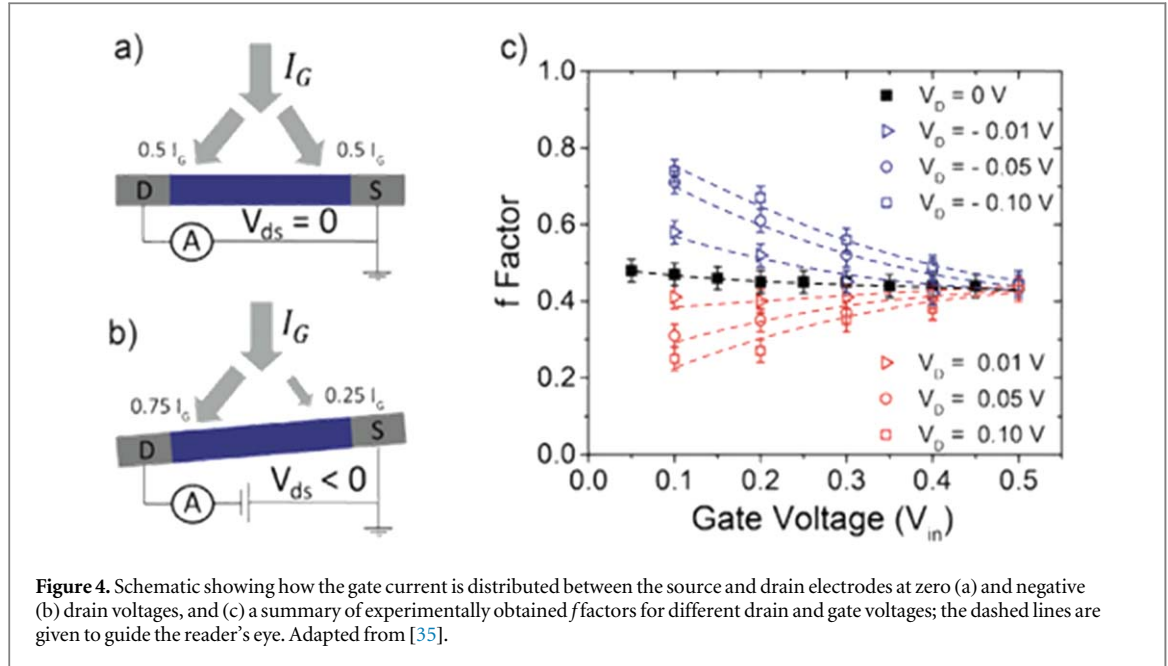
depend on the analyte concentration and can be estimated by using the Nerst equation or can be determined experimentally. The effective gate voltage is then incorporated in the B-M source-drain current expression (equations (10) and (11)), in order to describe the biosensor output characteristics.

3.1.2. Transient behavior

The transient state is defined as the operation mode of the transistor where the ionic current, which comes from the electrolyte upon a certain gate voltage application, still changes with time. In other words, the channel has been charged by ions, and doping or de-doping of the semiconducting material is still in progress. In this situation, Ohm's law, as described in equation (1), is no longer sufficient, and a time-dependent current contribution associated with the doping/de-doping process has to be added. Therefore, there will be two current contributions in the device: one coming from the injection of anions/cations from the electrolyte and another from the injection/removal of holes by the source electrode. For simplicity, the model ignores the spatial variation of the voltage and hole density, by assuming an average ionic current and hole density. Under these considerations, Ohm's law can be written as

$$J(t) = \frac{I(t)}{WT} \approx q\mu p(t)\frac{V_d}{L} + qfL\frac{dp(t)}{dt}, \qquad (12)$$

where $p(t)$ is the change in charge density with time, $\frac{V_d}{L}$ is the average electric field within the channel, and the f factor is a constant that accounts for the spatial nonuniformity of the doping/de-doping process. Basically, the ion flux coming from the electrolyte into the channel is split between the source and drain electrodes, depending on the magnitude of V_d and V_g. The fraction of this current that is captured by the ammeter at the drain electrode defines the factor f. Figure 4 below, adapted from [35], illustrates the

Figure 4. Schematic showing how the gate current is distributed between the source and drain electrodes at zero (a) and negative (b) drain voltages, and (c) a summary of experimentally obtained *f* factors for different drain and gate voltages; the dashed lines are given to guide the reader's eye. Adapted from [35].

origin of the *f* factor better. For $V_d = 0$, the drain and source electrodes are short circuited, and there is no preferential potential for ionic charges to follow. Therefore, the doping/de-doping of the channel is said to be uniform. That way, the *f* factor tends to the value of $\frac{1}{2}$. Conversely, when $V_d \neq 0$, there will be a preferable 'potential' path for ions to follow, and doping/de-doping of the semiconducting layer will be nonuniform along the channel. This situation is illustrated in figure 4(b). In figure 4(c), an in-depth calculation of the *f* factor is shown, using a PEDOT: PSS-based OECT, for various drain and gate voltages. The method for extracting the *f* factor will be detailed in section 4 of this review.

Using equation (2) for the depletion mode (or equation (3) for accumulation mode OECT), one can rewrite equation (12) as

$$I(t) = \frac{WT}{L} q\mu\rho_0 \left(1 - \frac{Q(t)}{q\rho_0 \nu}\right) V_d - f\frac{d(Q(t))}{dt}, \quad (13)$$

where $Q(t)$ is the number of ionic charges that the semiconducting channel uptakes over time. In this sub-section, we focus only on the development of an expression of the depletion-mode OECT. Although the transient state B-M model allows for a good estimation of semiconductors parameters, such as charge carrier mobility, the final expression does not completely fit the experimental drain currents. Moreover, it does not quantitatively extract useful device characteristics and ionic impedances. These were accomplished better by models that use equivalent circuits which are discussed in section 4.

The term $\frac{WT}{L} q\mu\rho_0 V_d$ in equation (13) can be assumed to be the initial source-drain current and is referred to as I_0. For further developments, the model assumes two independent types of measurements: constant gate current and constant gate voltage. The first measurement is not commonly used by the OECT

community but allows for an easy simplification of equation (13), which is given by the relation $\frac{dQ(t)}{dt} = I_g = \frac{Q(t)}{t}$. This assumption $I_g = \frac{Q(t)}{t}$, however, is an oversimplification and a source of possible errors that might lead to an inaccuracy in the model.

Assuming that the transit time of electronic charges is $\tau_e = L^2/\mu V_d$, V_d can be replaced in equation (13), and the expression takes the following form:

$$I(t) = I_0 - \mu\frac{V_d}{L^2}Q(t) - fI_g = I_0 - t\frac{I_g}{\tau_e} - fI_g. \quad (14)$$

Bernards and Malliaras applied this analytical expression to constant gate current measurements and were able to extract the transit time τ_e of their material with good agreement with the literature [32].

As for the constant gate voltage measurement, the model assumes that the ionic uptake by the channel follows the exponential characteristic of an ideal charging capacitor:

$$Q(t) = Q_{ss}(1 - e^{-\frac{t}{\tau_i}}), \quad (15)$$

where $\tau_i = R_s C_d$ is the charging time, with R_s being the electrolyte resistance and C_d being the total channel capacitance. Moreover, the steady-state charge Q_{ss} is equal to the product $C_d \Delta V$, where ΔV is the voltage applied across the electrolyte. Here, the B-M model uses a simplified ionic circuit. It has been well accepted that the ionic system in OECT devices can be captured using a three-element, equivalent circuit as shown in figure 6(c). It distinguishes itself from the ionic circuit used in the B-M model via the inclusion of a channel resistance R_d. Such resistance, known in the electrochemistry field as the charge-transfer resistance, accounts for the possibility of charge exchange between ionic species and the polymer backbone. It depends on the physical chemistry of

the materials as well as the nature of the solvent, ionic species, and device geometry.

As will be shown in section 4, the three-element, equivalent circuit gives a charging time as

$$\tau = \frac{C_d R_d R_s}{R_d + R_s}, \qquad (16)$$

which is different from that assumed in equation (15). Indeed, the B-M model characteristic time is valid only for the case in which $R_d \gg R_s$, which is often true for most PEDOT:PSS-based OECT device geometries and commonly used aqueous electrolyte concentrations (0.1–1 M). However, for new systems and miniaturized OECT geometries, such a limit might no longer be valid.

The model also assumes that de-doping occurs everywhere in the film without saturation effects. Because of that, the average voltage drop is assumed to be $\Delta V = V_g - \frac{1}{2}V_d$. Using this assumption, the transient expression can be simplified as follows:

$$I(t, V_g) \approx \mathrm{I}_{ss}(V_g) + \Delta I_{ss}\left(1 - f\frac{\tau_e}{\tau_i}\right)e^{-\frac{t}{\tau_i}}. \qquad (17)$$

For an in-depth algebraic development from equations (14)–(17), the reader is referred to the supplementary material, section A. Bernards and Malliaras used equation (17) mainly to qualitatively predict the decay and recovery characteristics of an OECT transient. The expression, however, did not allow for the extraction of quantitative parameters. This was only possible by using the equivalent circuit model which is reviewed in section 4.

3.2. B-M model with carrier concentration dependent mobility

Friedlein *et al* [34] further improved the original B-M model, accounting for the influence of charge carrier density ρ on the charge carrier mobility μ. They assumed a dependency of μ on ρ as was proposed by the seminal work of Vissenberg and Matters on the mobility in amorphous organic transistor [42]. In this work, the authors considered the density of states (DOS) to be of an exponential form

$$g(\epsilon) = \frac{N_t}{k_B T_0} e^{\left(\frac{\epsilon}{k_B \Theta_0}\right)}, \qquad (18)$$

where N_t is the number of states per unit volume, k_B is the Boltzmann's constant, and Θ_0 is a parameter that indicates the width of the exponential distribution. By assuming that the transport of charge carriers within the proposed DOS is governed by hopping of charge carriers between states, the model of Vissenberg and Matters suggests a field-effect mobility as follows:

$$\mu_{FE} = \mu_0 \rho_0 \left[\frac{\pi(\Theta_0/\Theta)^3}{(2\alpha)^3 B_c \Gamma(1 - \Theta/\Theta_0)\Gamma(1 + \Theta/\Theta_0)} \right]^{\frac{\Theta_0}{\Theta}}$$
$$\times \left[\frac{(CV_g)^2}{2k_B \Theta_0 \epsilon_s} \right]^{\frac{\Theta_0}{\Theta} - 1}. \qquad (19)$$

Here, μ_0 is a prefactor for mobility, ρ_0 is the zero-field charge concentration, α^{-1} is the effective overlap parameter between localized states, B_c is a dimensionless number related to the percolation of charges, Γ is the Gamma function, C is the device capacitance per unit of area, ϵ_s is the dielectric constant of the material, and Θ is the temperature [42, 56].

Based on this mobility dependence, Friedlein *et al* proposed a simplified mobility relation for the depletion mode as being [34]:

$$\mu(\rho) = \mu_0 \left(\frac{\rho}{\rho_0}\right)^{\frac{E_0}{k_B \Theta} - 1}. \qquad (20)$$

The development of the model follows the structure of the original B-M model: equations (2) and (20) are plugged into equation (1), yielding

$$J = q\mu_0 \rho_0 \left[1 - \frac{(V_g - V(x))}{V_p}\right]^{\frac{E_0}{k_B \Theta}} \frac{dV(x)}{dx}, \qquad (21)$$

which resembles equation (9), except for the prefactor μ_0 and the exponent $\frac{E_0}{k_B \Theta}$ which arise from equation (20). It is worth mentioning that this development is exclusively for depletion-mode OECT. An extension to accumulation mode OECT, however, is rather simple: one simply has to use equation (3) instead of equation (2) and follow the same mathematical steps.

The integration of equation (21) generates the final current–voltage relationship, which is valid until the saturation regime

$$I = \frac{q\mu_0 \rho_0 WT}{L} \frac{1}{\frac{E_0}{k_B \Theta} + 1} V_p \left[\left(1 - \frac{V_g - V_d}{V_p}\right)^{\frac{E_0}{k_B \Theta} + 1}\right.$$
$$\left. - \left(1 - \frac{V_g}{V_p}\right)^{\frac{E_0}{k_B \Theta} + 1}\right]. \qquad (22)$$

Friedlein *et al* used this model to fit experimental data and were able to successfully recreate the output characteristics of PEDOT:PSS-based OECTs. In fact, they compared the original B-M model with the non-uniform mobility model, see figure 5, which was adapted from the original publication [34]. The original B-M fits are presented in figures 5(a) and (c), whereas the nonuniform mobility model fits can be seen in figures 5(b) and (d). The fit quality of the latter is definitively higher and better reproduces the transition between the linear and saturation regime, where the original model tends to fail. This model provides ways
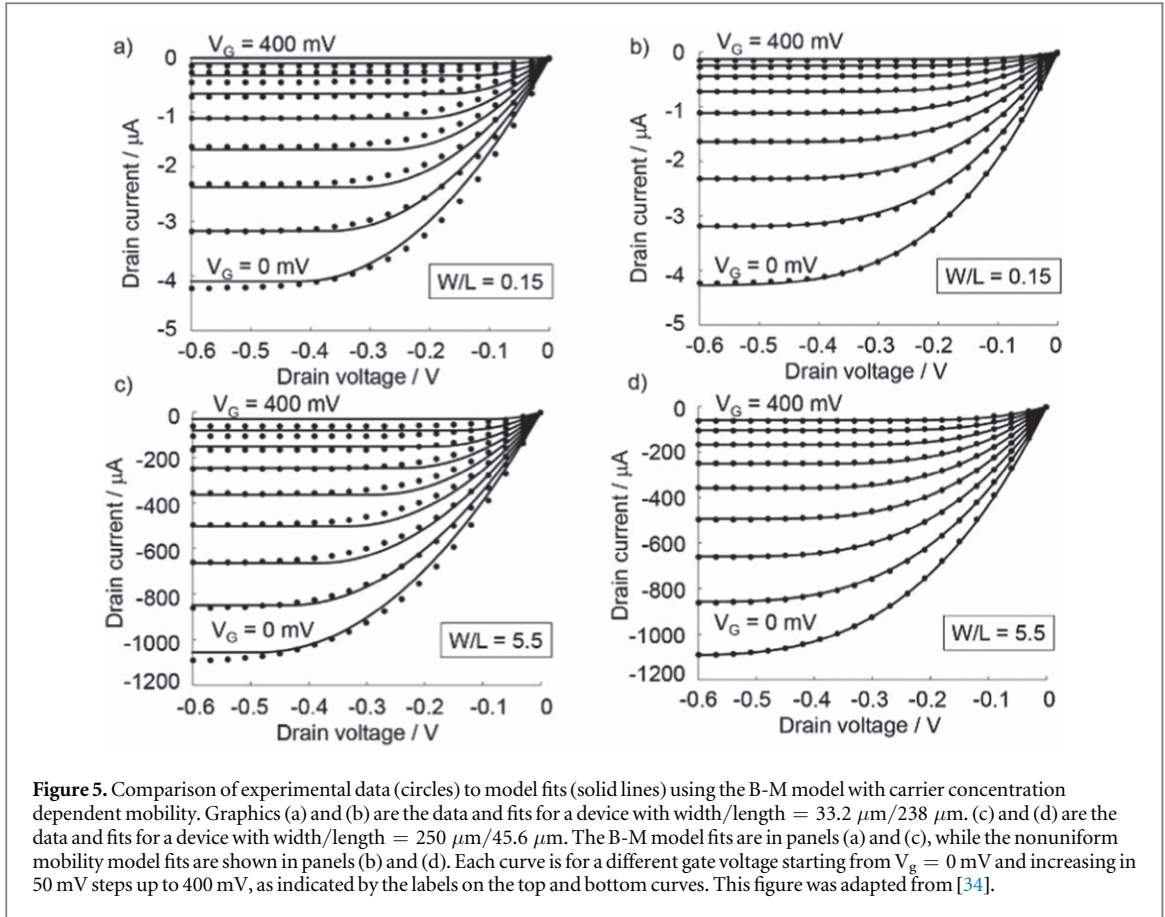
Figure 5. Comparison of experimental data (circles) to model fits (solid lines) using the B-M model with carrier concentration dependent mobility. Graphics (a) and (b) are the data and fits for a device with width/length = 33.2 μm/238 μm. (c) and (d) are the data and fits for a device with width/length = 250 μm/45.6 μm. The B-M model fits are in panels (a) and (c), while the nonuniform mobility model fits are shown in panels (b) and (d). Each curve is for a different gate voltage starting from V_g = 0 mV and increasing in 50 mV steps up to 400 mV, as indicated by the labels on the top and bottom curves. This figure was adapted from [34].

of calculating several parameters, such as the conductivity of the active material, the zero-field mobility as well as the disorder parameter, which can be associated with the material morphology.

Another interesting feature arising from the presented model is that the nonuniform mobility provides a substantially larger pinch-off voltage compared to those calculated through the original B-M model. This is an important result and can lead to a better understanding of how material parameters can be used to enhance the device output.

Finally, it is worth mentioning that the validity of equation (19) (or, similarly, equation (20)) for the non-uniformity of mobility in amorphous polymers is not completely accepted. For instance, the work by Campbell *et al* [57] suggested that the variable range hopping model field-effect mobility proposed by Vissenberg and Matters [42] are about three orders of magnitude higher than that experimentally measured by them. They have used two amorphous fluorene-triarylamine copolymers, and both led to the same discrepancy. Their experimental results suggest that the charge carrier mobility is independent of the charge carrier density, at least for the material they used. Therefore, it is important to the OECT community to promote fundamental progress in the understanding of the intricate mechanisms of conductivity in organic mixed conductors. For instance, a detailed study of the dependency of the mobility on the charge density in OECT devices is needed to further correct or verify the models reviewed in this section.
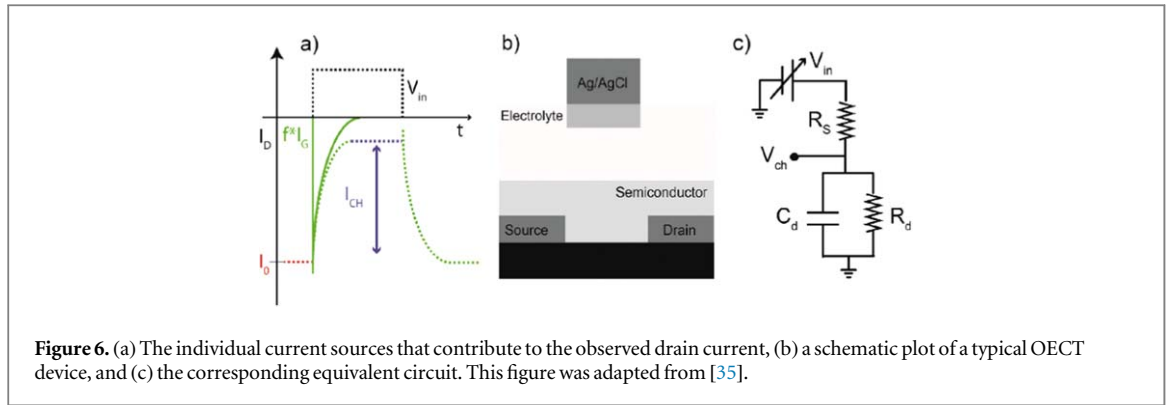
4. Equivalent circuit model

Another important group of theoretical models developed to describe drain-transient currents in OECTs are those based solely on equivalent circuits. Equivalent circuits have been extensively used as a useful tool in organic electronics to fit currents and impedance responses of a variety of devices within the field [58, 59]. Indeed, even OECT-based biosensors were studied and described by using complex equivalent circuit [40]. It was only in 2017, however, that a complete equivalent circuit model, including charge-transfer resistance, was developed. The model was not only able to fully predict the drain current in OECT devices upon application of a gate voltage but offered a rational way to experimentally determine the f factor introduced in equation (12), in section 3.1.2. The so-called Faria–Duong model [35] considers that the transient response of the drain current, $I_D(t)$, can be described by breaking it down into three contributing currents:

$$I_D(t) = I_0 - f^*I_G(t) + \Delta I_{ch}$$
$$= I_0 - f^*I_G(t) \pm g_m V_{ch}(t). \quad (23)$$

As before, I_0 is the drain-source current prior to application of a gate voltage and depends solely on the initial conductivity of the material and the device geometry. Note that in the depletion mode, I_0 is normally large. Contrarily, for accumulation mode OECT, I_0 is rather small and tends to be close to zero. Similarly as

Figure 6. (a) The individual current sources that contribute to the observed drain current, (b) a schematic plot of a typical OECT device, and (c) the corresponding equivalent circuit. This figure was adapted from [35].

in equation (12), f is the factor used to account for the spatial nonuniformity of the ionic uptake process, $I_G(t)$ is the gate current, ΔI_{ch} is the channel current, g_m is the transconductance, and V_{ch} is the channel potential relative to the ground.

Upon application of a gate voltage, a flux of ions will be generated in the electrolyte toward the polymer film giving rise to a time-dependent gate current $I_G(t)$. This current has an exponential form, similar to a capacitive charging process. Finally, ΔI_{ch} relates to the change in the conductivity, due to the doping/de-doping of the active polymer by oxidation/reduction of the channel. In figure 6(a), ΔI_{ch} leads to a steady-state current, that is related to the OECT ON/OFF ratio, being described by $\Delta I_{ch} = g_m V_{ch}(t)$, see equation (23). Here, g_m is the device transconductance which is given by $g_m = \frac{\Delta I_{DS}}{\Delta V_G}$. In the steady state V_{ch} is constant and tends to approach V_g when the electrolyte resistance is far smaller than the channel impedance. Obviously, during the transient process, V_{ch} changes over time, as has already been discussed in [40].

In equation (23), I_0 can be read directly from the experimental data as well as the device transconductance g_m. The gate current $I_G(t)$ and the channel potential $V_{ch}(t)$, however, have to be determined. The model calculates them by proposing an equivalent circuit that corresponds to a typical OECT structure. The schematic design of an OECT is shown in figure 6(b) side-by-side with the proposed circuit, depicted in figure 6(c).

The circuit is composed of a resistor R_d and a capacitor C_d representing the transistor channel, while R_s represents the resistance of the electrolyte solution (figure 6(c)). As mentioned before, R_d is related to the possibility of a charge transfer between the ionic species and the polymer backbone. Given that the ion tends to be surrounded by solvent molecules, the latter forms an insulating dielectric around the ionic species, and therefore, R_d tends to be in the orders of kΩ to MΩ, depending on the nature of the solvent, the ionic species, the polymer, as well as the device geometry.

In order to determine I_G and V_{CH}, the authors of [35] made use of a commonly utilized method to solve complex circuits. The method is the Laplace transform for circuit analyses and basically converts impedance circuits with voltage and current signals that change with time to the so-called s-domain (similar to a frequency space) [60]. In doing so, the circuit that would require the solution of elaborated differential equations in the time domain will only require manipulation of an algebraic equation. Finally, to reestablish the time-domain response, the inverse of the Laplace transform is applied.

The frequency-space impedances of this equivalent circuit illustrated in figure 6(c) becomes

$$Z_s = R_s \tag{24}$$

for the electrolyte portion and

$$Z_d = \frac{R_d}{1 + s(R_d C_d)} \tag{25}$$

for the device impedance. Using Ohm's and Kirchoff's laws, I_G and V_{CH} are then calculated as follows:

$$V_{ch} = \frac{Z_d}{Z_s + Z_d} V_G(s) \tag{26}$$

$$I_G = \frac{1}{Z_s + Z_d} V_G(s). \tag{27}$$

Here, $V_G(s)$ is the time-dependent gate voltage in the s-domain. Given that pulsed gate measurement is the most common transient measurement in OECT, V_G can be represented by a simple Heaviside function with an amplitude of V_0. By performing an inverse Laplace transform on equations (26) and (27) and plugging the results into equation (23), it is possible to obtain the drain current of an OECT, as shown in equation (28) below. In the supplementary material, section B, we provide a simple Mathematica code to calculate equations (26) and (27). Note that the drain current is only dependent on the device resistance, capacitance, and transconductance, as well as the gate voltage strength:
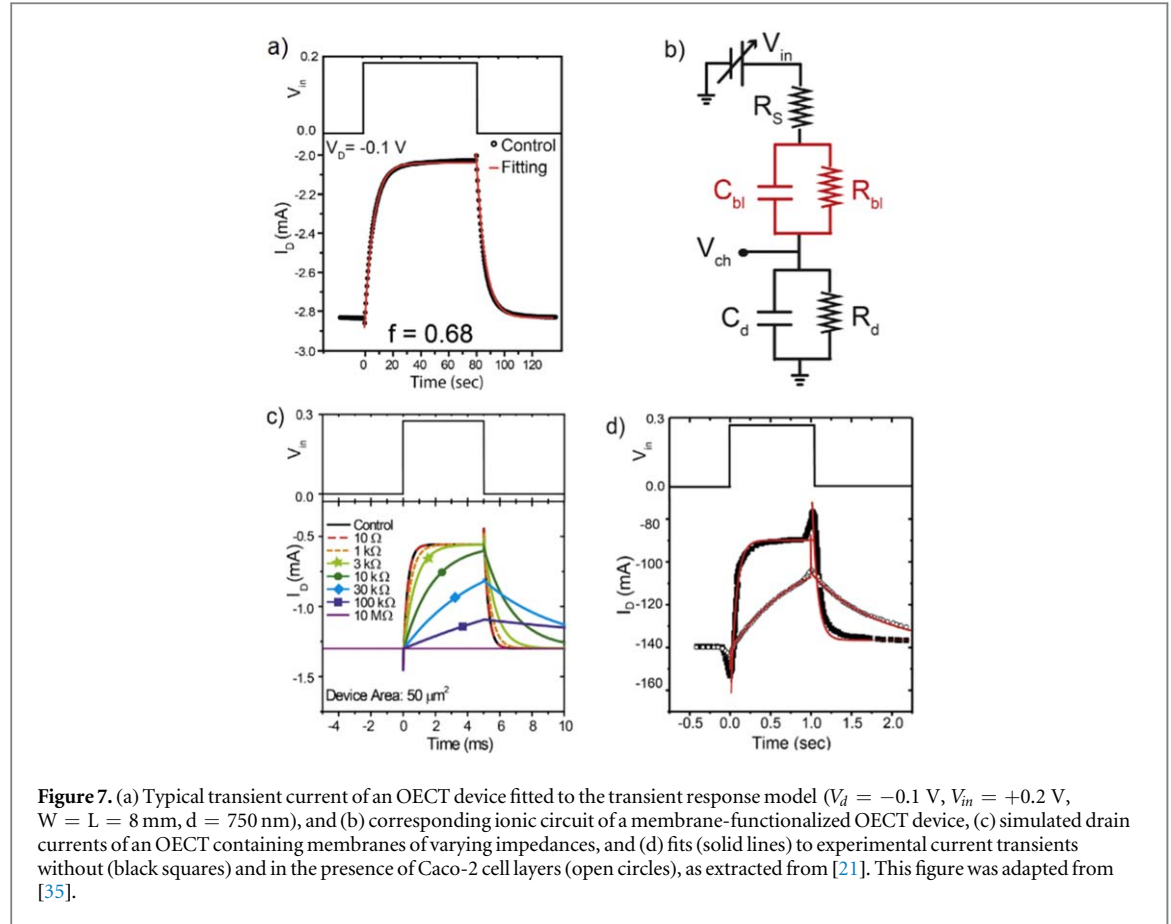
Figure 7. (a) Typical transient current of an OECT device fitted to the transient response model ($V_d = -0.1$ V, $V_{in} = +0.2$ V, W = L = 8 mm, d = 750 nm), and (b) corresponding ionic circuit of a membrane-functionalized OECT device, (c) simulated drain currents of an OECT containing membranes of varying impedances, and (d) fits (solid lines) to experimental current transients without (black squares) and in the presence of Caco-2 cell layers (open circles), as extracted from [21]. This figure was adapted from [35].

$$I_D(t) = I_0 + \frac{V_0(g_m R_d - f)}{R_d + R_s} - \frac{V_0 R_d(g_m R_s + f)}{R_s(R_d + R_s)}$$
$$\times\, e^{\left(-\frac{R_d + R_s}{C_d R_d R_s}t\right)}. \tag{28}$$

The characteristic charging time τ of the device can now be assigned as $\tau = \frac{C_d R_d R_s}{R_d + R_s}$. As it would be expected, the exponential law assumes a single time constant. When $R_d \gg R_s$, which is true for a variety of OECT devices (macroscopic channel geometry and high electrolyte concentrations), τ reduces to $C_d R_s$ (similar to the value used in the B-M transient model).
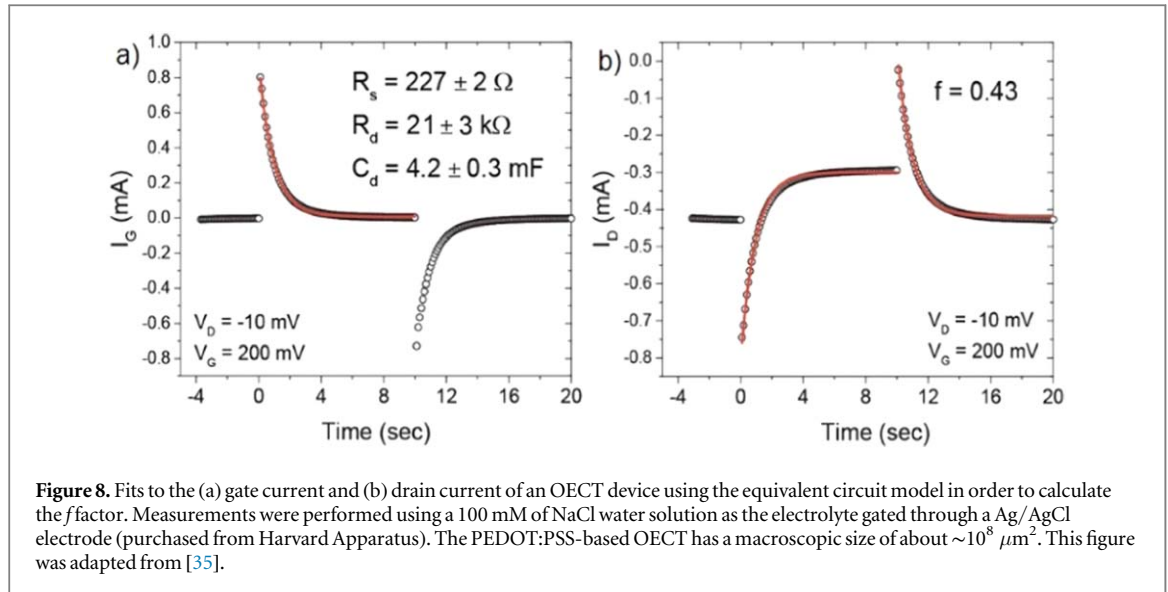
The authors successfully applied equation (28) to describe the drain-transient current of a regular PEDOT:PSS-based OECT. The experimental data (dots) and the fitting curve (red line) are shown in figure 7(a). The device geometry and details can be found in the figure caption. The fit yields circuit parameters of $R_s = (1.9 \pm 0.5)$ $k\Omega$, $R_d = (150 \pm 20)$ $k\Omega$ and $C_d = (2.7 \pm 0.3)$ mF with an R^2 of 0.998. From this, a volumetric capacitance of 56 Fcm^{-3} can be calculated, which is in good agreement with the literature [6].

The model was also extended to describe a membrane-functionalized OECT. This is especially useful to the OECT biosensing community which often incorporate biological membranes on the transistor channel. Such membranes can partially block ionic species. Therefore, the accumulation of ions between the membrane forms an extra capacitive response to the device. Besides, ions can also penetrate through the membrane, characterizing a resistance for ionic fluxes. Therefore, such membranes can be accounted for in the model by adding an extra circuit loop containing a resistor R_{bl} and capacitor C_{bl} to represent the blocking membrane layer. This will form a five-element circuit model, as shown in figure 7(b). It can be solved using the same method applied to the non-functionalized OECT. The original manuscript, along with its supplementary material, explains the detailed development of the five-element circuit model. Because the circuit has two RC loops, the final drain current response for a membrane-functionalized OECT consists of two exponential forms with distinct time constants:

$$I_D(t) = A + B_1 \exp\left(-\frac{t}{\tau_1}\right) - B_2 \exp\left(-\frac{t}{\tau_2}\right). \tag{29}$$

The first time constant τ_1 represents the charging time of the polymer channel, whereas the second one τ_2 corresponds to the charging time of the blocking membrane layer. Normally the device capacitance is greater than that of the biological membrane, and therefore, τ_1 is typically larger than τ_2. Expressions for A, B_1, B_2, τ_1, and τ_2 as a function of resistances, capacitances, and gate voltage amplitude can be found in the supporting information, section B, or in the original manuscript by Faria *et al* [35].

Figure 8. Fits to the (a) gate current and (b) drain current of an OECT device using the equivalent circuit model in order to calculate the *f* factor. Measurements were performed using a 100 mM of NaCl water solution as the electrolyte gated through a Ag/AgCl electrode (purchased from Harvard Apparatus). The PEDOT:PSS-based OECT has a macroscopic size of about $\sim 10^8$ μm^2. This figure was adapted from [35].

As demonstrated in figure 7(c), equation (29) was used to predict drain-transient responses for membranes of varying impedances using device characteristics extracted from [11] and [61]. The device and membrane impedances, as well as the potentials used, were the following: $R_s = 1.8$ kΩ, $R_d = 18$ MΩ, $C_d = 150$ nF, $R_{bl} = 10$ kΩ cm^2, $C_{bl} = 1$ μF cm^{-2}, a gate voltage amplitude of 0.275 V and drain voltage of -0.6 V. The numbers for the membrane are the typical values for supported lipid bilayers. The simulated current shows very good similarities to those experimentally measured, where the impedance of the functionalized membrane reduces the device switching speed, which is supported by previously published OECT biosensing results [20, 21, 62].

Finally, the authors applied their model to fit experimental results from a previously published work by Jimison *et al* in monitoring the integrity of Caco-2 tissue barriers [21]. Caco-2 are epithelial cells that present a tight junction that maintains the integrity of the cell layer. Bacteria or other harsh substances disrupt the tight junctions and destroy the cohesion of the cell layer. Jimison *et al* built a real-time OECT biosensor to monitor the ion-blocking properties of the cell layer when exposed to toxic compounds. With the help of equation (28), they fitted the non-functionalized OECT, see figure 7(d), obtaining the following circuit parameters: $R_s = (4.6 \pm 0.4)$ kΩ, $R_d = (1.4 \pm 0.4)$ MΩ, and $C_d = (14.1 \pm 0.6)$ μF. Hence, using those impedances and equation (29), they fitted the same OECT, however, with cell layers added to the channel. The second fit yields membrane impedances of $R_{bl} = (50.7 \pm 0.8)$ kΩ and $C_{bl} = (420 \pm 50)$ nF.

Finally, it is important to mention that this model offers a simple way to calculate the spatial non-uniformity of the ion uptake process, i.e., the *f* factor. This is often important, even when using the B-M transient model. To calculate the *f* factor, it is

necessary to measure both the drain and the gate transient currents simultaneously. This is experimentally easy to accomplish, and it is often done using a dual-channel source meter. Figures 8(a) and (b) illustrate both the gate and drain-transient current measured simultaneously from the same device (device details can be found in the figure caption).

First, it is necessary to fit the gate current, which is independent of the *f* factor. This can be done using the following equation:

$$I_g(t) = \frac{V_0}{R_d + R_s} + \frac{V_0 R_d}{R_s(R_d + R_s)} e^{\left(-\frac{R_d + R_s}{C_d R_d R_s}t\right)}. \quad (30)$$

This expression was obtained by calculating the inverse of the Laplace transform of equation (27). The fit yields impedances for the OECT device including R_s, R_d, and C_d, as shown in the inset of figure 8(a). Using the impedance parameters from the prior fitting, the drain-transient response is then fitted via equation (28), where now the *f* factor is the only fit parameter, as illustrated in figure 8(b). As already mentioned, the *f* factor depends on the drain and gate voltages. The graph in figure 4(c) was built using the aforementioned method.

Although the model allows to fully recreate the drain-transient responses of both plain and membrane-functionalized OECTs, it has few deficiencies. First, the model does not take into consideration aspects of the electronic conductivity. For instance, details of the charge carrier density or the mobility are not included in the model. A way to overcome such simplifications is to combine this model with aspects of the B-M proposal. Second, the work by Rivnay *et al* suggests the ionic penetration in amorphous and crystalline portions of PEDOT:PSS films respond in different time scales [63]. Given that the crystalline domains have a denser microstructure than the amorphous region, ions do take longer to swell the former, responding in a slower characteristic time. In the current model, the authors associate a single ideal

capacitor to represent the intricate polymer bulk. It might be necessary to incorporate a more elaborated/realistic equivalent circuit, maybe adding a constant phase element to it [64, 65]. Indeed, Gentile *et al* proposed a model that could partially overcome those deficiencies [36]. This model will be discussed in section 5.

Still in equivalent circuit models, Friedlein *et al* have also proposed an interesting development assuming a simplified RC series circuit, allowing for an unequal drain current assuming an ideal FET transistor in between the drain and source [33]. They also used a similar calculation method, as discussed in the Faria–Duong model (Laplace/Fourier transform) to calculate both the gate and channel transient current. In the Friedlein model, it is assumed that a voltage step is applied on the top of a DC offset voltage. They use their model to describe drain-transient response with a time constant that is about 30 times faster than the ionic speed meaning the channel charging time constant. This interesting feature takes place in a very particular combination of V_D and V_g. In fact, the so-called 'faster-than-ionic' response is basically an optimal superposition of the gate current spike and the channel current. In this situation, the gate current, at very short times, is fundamentally given by the displacement current, i.e., $I_{disp} = C_d \frac{dV(t)}{dt}$, and dominates the initial current spike normally seen in OECT transient responses. As the capacitor starts to be charged, I_g decays. If the strength of the channel current I_{ch} is such that its superposition with I_g produces a perfect square function, the device will reach its saturation current in a time interval smaller than the ionic response. Note that this optimal superposition will only happen when I_g and I_{ch} rise in the same direction.

This is illustrated in figure 9. While figures 9(a) and (c) present the change in the source current upon a step voltage applied to the gate, figures 9(b) and (d) show the corresponding gate and channel currents separately. Although the measurements are done using exactly the same PEDOT:PSS-based OECT, the charging time in figure 9(a) is 30 times slower than that of figure 9(c).

5. Hybrid models: B-M model with an equivalent circuit

Gentile *et al* proposed a hybrid B-M-equivalent circuit model in order to describe the transient response of OECTs better [36]. The proposed equivalent circuit is similar to the one illustrated in figure 6(c), with the difference that a Warburg impedance element Z_w was used instead of a simple charge-transfer resistance R_d. In OECTs, such impedance may account for the diffusion response of different ionic species. The Warburg impedance is a complex valued quantity given by [66]

$$Z_w = A_w \left[\frac{1}{\sqrt{\omega}} - i\frac{1}{\sqrt{\omega}} \right], \qquad (31)$$

where A_w is known as the Warburg coefficient and i is the imaginary number. A_w is related to the diffusion coefficient through the relation

$$A_w = \frac{R\Theta}{n^2 F^2 A c_0} \sqrt{\frac{1}{2D}}. \qquad (32)$$

Here, R is the universal gas constant, Θ is the temperature, n is the number of charges involved in the process, F is the Faraday constant, A is the interfacial area between the polymer and the electrolyte, c_0 is the initial charge concentration, and finally, D is the molecular diffusion coefficient of ions. Proceeding with the calculation of the equivalent impedance generates the following equation:

$$Z_{eq} = R_s + \frac{A_W}{\sqrt{\omega} + 2C_{DL}\omega A_W{}^2 + 2C_{DL}{}^2 A_W{}^2 \omega^{3/2}}$$
$$- i \left[\frac{A_W(2C_{DL}A_W + 1/\sqrt{\omega})}{1 + 2C_{DL}A_W\sqrt{\omega} + 2C_{DL}{}^2 A_W{}^2 \omega} \right]. \qquad (33)$$

For details on calculating Z_{eq}, the reader is referred to the supplementary material, section C.

The total amount of charge exchanged between the electrolyte and the polymer film can then be calculated using

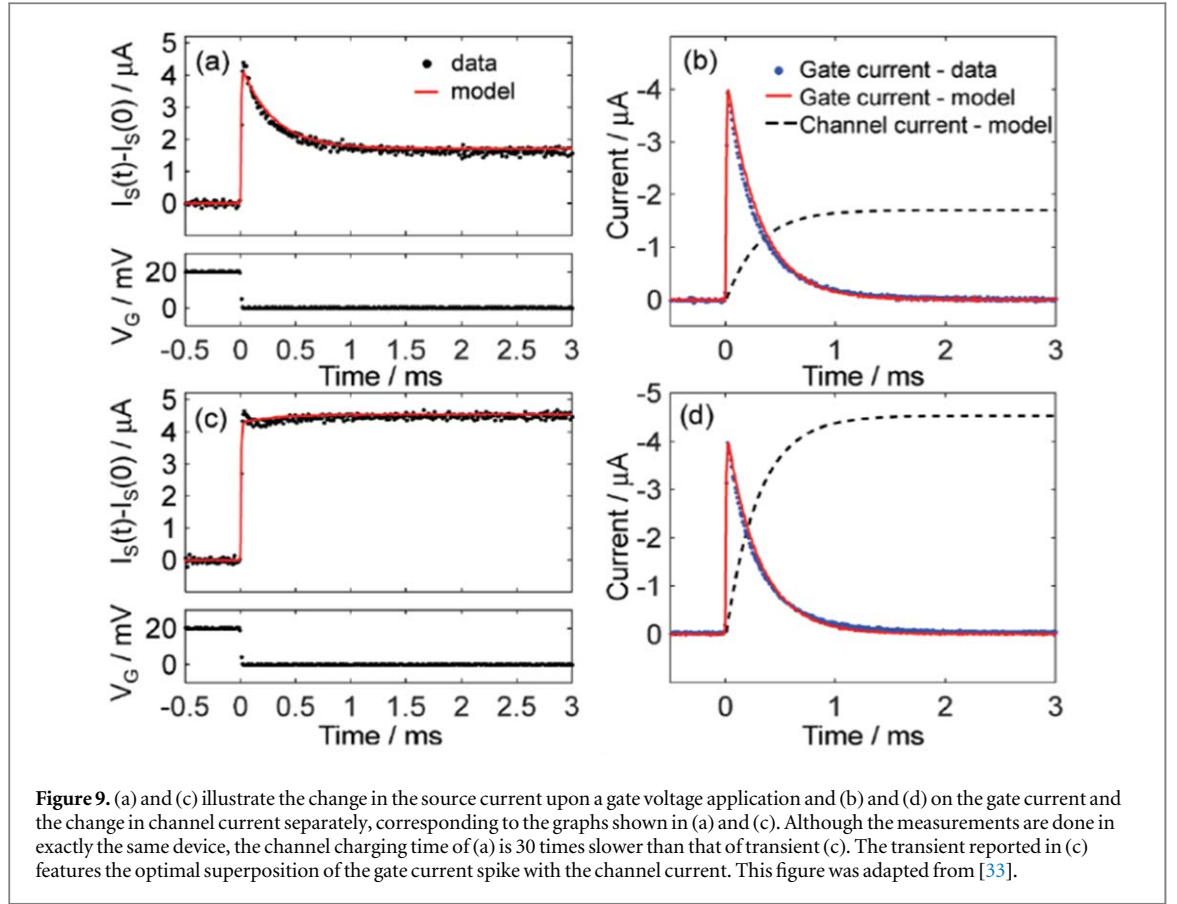$$Q(t) = \int_0^t \frac{\varphi(t)}{|Z_{eq}|} dt, \qquad (34)$$

where $\varphi(t)$ is the time-dependent gate voltage. Here, the authors have chosen a triangular gate voltage, although such stimulation in the gate electrode is usually not used to characterize the transient response of OECTs. Finally, the time-dependent drain current is calculated by plugging equation (34) into equation (13). Moreover, in their work, Gentile *et al* assume that the f factor is expressed by the following relation:

$$f \sim \frac{\sqrt{\frac{D}{f_{Hz}}}}{T}, \qquad (35)$$

where f_{Hz} is the input voltage frequency and T is the film thickness [36]. The authors refer to this ratio as the penetration depth of ions into the organic film. It is worth mentioning that the origin of the f factor is most probably due to the spatial voltage profile across the transistor channel, due to the application of a simultaneous V_D and V_g potentials, see figure 4.

Solving the combination of equation (13) with equations (33) and (34) yields an expression to the drain-transient current. The authors applied the derived expression for a series of OECT measurements using a triangular gate voltage stimulus with varying frequencies. Their fit shows good agreement with experimental data. The authors claim that their model is sensitive to capture the response of individual ionic species, and therefore, allows discriminating the type of salt used.

Figure 9. (a) and (c) illustrate the change in the source current upon a gate voltage application and (b) and (d) on the gate current and the change in channel current separately, corresponding to the graphs shown in (a) and (c). Although the measurements are done in exactly the same device, the channel charging time of (a) is 30 times slower than that of transient (c). The transient reported in (c) features the optimal superposition of the gate current spike with the channel current. This figure was adapted from [33].

6. Drift-diffusion-based models

The OECT models discussed so far mainly originate from Ohm's law (equation (1)) where the charge density ρ and the charge carrier mobility μ are modeled to describe experimentally measured data. In addition to this ohmic term, part of the current density J may arise from diffusion of charges. Taking this phenomenon into account, several elaborated models have been introduced in recent years [27–29, 31] to describe OECTs. In order to present a more complete review, in this section we briefly summarize the most important and recent ones among them.

The so-called diffusion current is the motion of carriers species due to the nonuniform density within the semiconductor layer and the electrolyte. Mathematically the current density J is expressed by

$$J = \sum_i J_i = \sum_i (q_i \mu_i \rho_i \boldsymbol{E} - D_i \nabla \rho_i), \qquad (36)$$

where, as before, q_i, μ_i, and ρ_i denote the charge ($-e$ for anions and $+e$ for holes and cations), the mobility, and the concentration, respectively. Here, however, the index i addresses the different potential charge carriers: holes, anions, and cations. The additional parameters D_i denote the diffusion coefficients of each of these species and can be related to the mobility via Einstein's relation [27]. In addition to equation (36), the continuity equation

$$\nabla J_i + \frac{\partial \rho_i}{\partial t} = 0 \qquad (37)$$

has to be fulfilled for each species i. Note that the quantities μ_i, D_i, and ρ_i in equations (36) and (37) depend on the spatial coordinate and are particularly different in the electrolyte and polymer regions. Solving the equations utilizing further physically motivated simplifications and assumptions as well as proper boundary conditions allows modeling the characteristics of electrochemical devices for both steady and transient states.

One of the first works which utilize a drift-diffusion based approach to model electrochemical devices was published by Prigodin *et al* [27]. In this work, the authors applied analytical attempts to solve the equations and considered screening, charging, and gating effects in the steady-state regime. They obtained expressions for an OECT which qualitatively resembles the source-drain IV characteristics for small ion concentrations. Their model, however, results in a sharp exponential dependence of the hole conductance with the gate voltage, which does not agree with experimental measurements.

An analytical study of the transient behavior of an OECT was published by Coppedè *et al* [31]. In their work, they solved equations (36) and (37) in one dimension using standard boundary conditions in conjunction with equations (2) and (12) from the B-M model. In doing so, the diffusion coefficients of different metal cations could be fitted to experimental

transient measurement with a very good agreement. Their method allows differentiating and distinguishing different molecules from a complex mixture, based on their diffusivity. In their work, however, only the ions in the electrolyte are considered.

In a more recent work, Tybrandt *et al* proposed consideration of both holes and ions with distinct electrostatic potentials for each of them which are coupled through Poisson's equation [28]. They argue that, since ionic and electronic charges exist in different phases, they are spatially separated and should, therefore, be modeled as an electronic double layer rather than a homogeneous phase. Their model enabled them to describe the charging behavior of polymer/electrolyte blends, the IV characteristics of OECTs, and the dynamic response of an electrolyte with great agreement to the experimental measurements.

Whereas most of the drift-diffusion based models are one dimensional, Szymanski *et al* formulated the first simulations on an OECT using a 2D model [29]. In this way, they were able to simulate a device architecture that is closer to real devices. While for steady-state mode, the dimension perpendicular to the source-drain direction does not play an important rule, it might be of importance for the transient mode, since regions away from the polymer–electrolyte interface experience different doping concentrations than those close to it. Thus, the 2D model might be a better approach to simulate both impedance spectroscopy and pulsed measurement. Furthermore, they were also able to study the influence of channel scaling on device performance.

It should be mentioned at this point that most of the drift-diffusion based models exhibit differential equations, the solutions of which are analytically not accessible without major simplifications. Hence, finite element methods are commonly used to solve these equations which may require high computational resources. Moreover, we would like to state that the diffusion coefficient is often used as a fit parameter to reproduce experimental data. To date, there are no attempts to simulate the diffusion behavior of ions at an atomic level. For a deeper understanding, it might be helpful to study the motion of atomic or molecular ions in a polymer matrix, for instance, based on molecular dynamics simulations.

7. Conclusions

OECTs have become a well-established standard device for application in several branches within electronics and bioelectronics. Understanding the device working mechanism and the fundamentals behind the ion–electron transduction mechanisms is the key to rational and fast device optimization. Here, we offered an in-depth review of several seminal works on modeling both the steady state and transient response regimes of OECTs. Giving that the

bioelectronics community is highly multidisciplinary, our first intention was to clarify most of the mathematical and physical developments and make the models accessible for everyone in the field. We have also discussed the pros and cons of the models reviewed within, and in the case of the B-M model, have extended their framework to the accumulation mode OECTs as well. We expect that this review contributes to show the beauty behind the device physics of OECTs and stimulate more and more scientists to contribute and further promote the understanding of OECTs and electrochemical-based devices alike.

ORCID iDs

Gregório Couto Faria ⓘ https://orcid.org/0000-0001-6138-8473

References

[1] Simon D T, Gabrielsson E O, Tybrandt K and Berggren M 2016 Organic bioelectronics: bridging the signaling gap between biology and technology *Chem. Rev.* **116** 13009–41

[2] Rivnay J, Owens R M and Malliaras G G 2014 The rise of organic bioelectronics *Chem. Mater.* **26** 679–85

[3] van de Burgt Y, Lubberman E, Fuller E J, Keene S T, Faria G C, Agarwal S, Marinella M J, Alec Talin A and Salleo A 2017 A non-volatile organic electrochemical device as a low-voltage artificial synapse for neuromorphic computing *Nat. Mater.* **16** 414–8

[4] Paulsen B D, Tybrandt K, Stavrinidou E and Rivnay J 2019 Organic mixed ionic–electronic conductors *Nat. Mater.* **19** 13–26

[5] Malti A *et al* 2015 An organic mixed ion-electron conductor for power electronics *Adv. Sci.* **3** 1–9

[6] Inal S, Malliaras G G and Rivnay J 2017 Benchmarking organic mixed conductors for transistors *Nat. Commun.* **8** 1767

[7] Riess I 2003 Mixed ionic-electronic conductors—material properties and applications *Solid State Ionics* **157** 1–17

[8] Rivnay J, Inal S, Salleo A, Owens R M, Berggren M and Malliaras G G 2018 Organic electrochemical transistors *Nat. Rev. Mater.* **3** 17086

[9] Park S *et al* 2018 Self-powered ultra-flexible electronics via nano-grating-patterned organic photovoltaics *Nature* **561** 516–21

[10] Fu Y, Kong L A, Chen Y, Wang J, Qian C, Yuan Y, Sun J, Gao Y and Wan Q 2018 Flexible neuromorphic architectures based on self-supported multiterminal organic transistors *ACS Appl. Mater. Interfaces* **10** 26443–50

[11] Rivnay J *et al* 2015 High-performance transistors for bioelectronics through tuning of channel thickness *Sci. Adv.* **1** e1400251–1400251

[12] Fan J, Montemagno C and Gupta M 2019 3D printed high transconductance organic electrochemical transistors on flexible substrates *Org. Electron.* **73** 122–9

[13] Sinha S K, Noh Y, Reljin N, Treich G M, Hajeb-Mohammadalipour S, Guo Y, Chon K H and Sotzing G A 2017 Screen-printed PEDOT:PSS electrodes on commercial finished textiles for electrocardiography *ACS Appl. Mater. Interfaces* **9** 37524–8

[14] Colucci R, Quadros M H, Feres F H, Maia F B, de Vicente F S, Faria G C, Santos L F and Gozzi G 2018 Cross-linked PEDOT:PSS as an alternative for low-cost solution-processed electronic devices *Synth. Met.* **241** 47–53

[15] Bihar E, Deng Y, Miyake T, Saadaoui M, Malliaras G G and Rolandi M 2016 A disposable paper breathalyzer with an alcohol sensing organic electrochemical transistor *Sci. Rep.* **6** 27582

[16] Hai W, Goda T, Takeuchi H, Yamaoka S, Horiguchi Y, Matsumoto A and Miyahara Y 2018 Human influenza virus detection using sialyllactose-functionalized organic electrochemical transistors *Sensors Actuators B* **260** 635–41

[17] Parlak O, Keene S T, Marais A, Curto V F and Salleo A 2018 Molecularly selective nanoporous membrane-based wearable organic electrochemical device for noninvasive cortisol sensing *Sci. Adv.* **4** 1–10

[18] Yang A, Li Y, Yang C, Fu Y, Wang N, Li L and Yan F 2018 Fabric organic electrochemical transistors for biosensors *Adv. Mater.* **30** 1–8

[19] Gentili D *et al* 2018 Integration of organic electrochemical transistors and immuno-affinity membranes for label-free detection of interleukin-6 in the physiological concentration range through antibody-antigen recognition *J. Mater. Chem. B* **6** 5400–6

[20] Pitsalidis C, Pappa A-M, Porel M, Artim C M, Faria G C, Duong D D, Alabi C A, Daniel S, Salleo A and Owens R M 2018 Biomimetic electronic devices for measuring bacterial membrane disruption *Adv. Mater.* **30** 1803130

[21] Jimison L H, Tria S A, Khodagholy D, Gurfinkel M, Lanzarini E, Hama A, Malliaras G G and Owens R M 2012 Measurement of barrier tissue integrity with an organic electrochemical transistor *Adv. Mater.* **24** 5919–23

[22] Khodagholy D *et al* 2013 *In vivo* recordings of brain activity using organic transistors *Nat. Commun.* **4** 1575

[23] Duong D T D T, Tuchman Y, Chakthranont P, Cavassin P, Colucci R, Jaramillo T F T F, Salleo A and Faria G C G C 2018 A universal platform for fabricating organic electrochemical devices *Adv. Electron. Mater.* **1800090** 1800090

[24] Gkoupidenis P, Schaefer N, Garlan B and Malliaras G G 2015 Neuromorphic functions in PEDOT:PSS organic electrochemical transistors *Adv. Mater.* **27** 7176–80

[25] Prigodin V N, Hsu F C, Kim Y M, Park J H, Waldmann O and Epstein A J 2005 Electric field control of charge transport in doped polymers *Synth. Met.* **153** 157–60

[26] Robinson N D, Svensson P-O, Nilsson D and Berggren M 2006 On the current saturation observed in electrochemical polymer transistors *J. Electrochem. Soc.* **153** H39

[27] Prigodin V N, Hsu F C, Park J H, Waldmann O and Epstein A J 2008 Electron-ion interaction in doped conducting polymers *Phys. Rev. B* **78** 035203

[28] Tybrandt K, Zozoulenko I V and Berggren M 2017 Chemical potential-electric double layer coupling in conjugated polymer-polyelectrolyte blends *Sci. Adv.* **3** 1–7

[29] Szymanski M Z, Tu D and Forchheimer R 2017 2D drift-diffusion simulation of organic electrochemical transistors *IEEE Trans. Electron Devices* **64** 5114–20

[30] Sideris P, Siskos S and Malliaras G 2017 Verilog-A modeling of organic electrochemical transistors *2017 6th Int. Conf. Mod. Circuits Syst. Technol. MOCAST* (IEEE) pp 3–6

[31] Coppedè N, Villani M and Gentile F 2014 Diffusion driven selectivity in organic electrochemical transistors *Sci. Rep.* **4** 4297

[32] Bernards D A and Malliaras G G 2007 Steady-state and transient behavior of organic electrochemical transistors *Adv. Funct. Mater.* **17** 3538–44

[33] Friedlein J T, Donahue M J, Shaheen S E, Malliaras G G and McLeod R R 2016 Microsecond response in organic electrochemical transistors: exceeding the ionic speed limit *Adv. Mater.* **28** 8398–404

[34] Friedlein J T, Shaheen S E, Malliaras G G and McLeod R R 2015 Optical measurements revealing nonuniform hole mobility in organic electrochemical transistors *Adv. Electron. Mater.* **1** 1500189

[35] Faria G C, Duong D T and Salleo A 2017 On the transient response of organic electrochemical transistors *Org. Electron.*. **45** 215–21

[36] Gentile F, Delmonte D, Solzi M, Villani M, Iannotta S, Zappettini A and Coppedè N 2016 A theoretical model for the time varying current in organic electrochemical transistors in a dynamic regime *Org. Electron.* **35** 59–64

[37] Shirinskaya A, Horowitz G, Rivnay J, Malliaras G G and Bonnassieux Y 2018 Numerical modeling of an organic electrochemical transistor *Biosensors* **8** 103–16

[38] Proctor C M, Rivnay J and Malliaras G G 2016 Understanding volumetric capacitance in conducting polymers *J. Polym. Sci. B* **54** 1433–6

[39] Kim S M *et al* 2018 Influence of PEDOT:PSS crystallinity and composition on electrochemical transistor performance and long-term stability *Nat. Commun.* **9** 3858

[40] Faria G C, Duong D T, Polyzoidis C A, Logothetidis S, Rivnay J, Owens R, Malliaras G G and Salleo A 2014 Organic electrochemical transistors as impedance biosensors *MRS Commun.* **4** 189–94

[41] Zaumseil J and Sirringhaus H 2007 Electron and ambipolar transport in organic field-effect transistors *Chem. Rev.* **107** 1296–323

[42] Vissenberg M C J M and Matters M 1998 Theory of the field-effect mobility in amorphous organic transistors *Phys. Rev. B* **57** 12964–7

[43] Faria G C, Faria R M, Deazevedo E R and Von Seggern H 2011 Temperature dependence of the drift mobility of poly(9,9′-dioctylfluorene- co -benzothiadiazole)-based thin-film devices *J. Phys. Chem. C* **115** 25479–83

[44] Santos L F, Faria R M, de Andrade A R, Faria G C, Amorin C A and Mergulhão S 2007 Transition from dispersive to non-dispersive transport of holes in poly(2-methoxy-5-(2′-ethyl-hexyloxy)-1,4-phenylene vinylene) light-emitting diodes investigated by time of flight measurements *Thin Solid Films* **515** 8034–9

[45] Bässler H 1993 Charge transport in disordered organic photoconductors: a Monte Carlo simulation study *Phys. Status Solidi* **175** 15–56

[46] Nilsson D, Robinson N, Berggren M and Forchheimer R 2005 Electrochemical logic circuits *Adv. Mater.* **17** 353–8

[47] Bernards D A, Malliaras G G, Toombes G E S and Gruner S M 2006 Gating of an organic transistor through a bilayer lipid membrane with ion channels *Appl. Phys. Lett.* **89** 053505

[48] Inal S, Rivnay J, Leleux P, Ferro M, Ramuz M, Brendel J C, Schmidt M M, Thelakkat M and Malliaras G G 2014 A high transconductance accumulation mode electrochemical transistor *Adv. Mater.* **26** 7450–5

[49] Giovannitti A *et al* 2016 N-type organic electrochemical transistors with stability in water *Nat. Commun.* **7** 13066

[50] Venkatraman V, Friedlein J T, Giovannitti A, Maria I P, McCulloch I, McLeod R R and Rivnay J 2018 Subthreshold operation of organic electrochemical transistors for biosignal amplification *Adv. Sci.* **5** 1–7

[51] Savva A, Giovannitti A, Maria I P, Ohayon D, Rivnay J, McCulloch I, Uguz I, Inal S, Pappa A M and Owens R M 2018 Direct metabolite detection with an n-type accumulation mode organic electrochemical transistor *Sci. Adv.* **4** eaat0911

[52] Giovannitti A, Sbircea D, Inal S, Nielsen C B, Bandiello E, Hanifi D A, Sessolo M, Malliaras G G, McCulloch I and Rivnay J 2016 Controlling the mode of operation of organic transistors through side-chain engineering *Proc. Natl Acad. Sci.* **113** 12017–22

[53] Mariani F, Conzuelo F, Cramer T, Gualandi I, Possanzini L, Tessarolo M, Fraboni B, Schuhmann W and Scavetta E 2019 Microscopic determination of carrier density and mobility in working organic electrochemical transistors *Small* **15** 1902534

[54] Bernards D A, MacAya D J, Nikolou M, Defranco J A, Takamatsu S and Malliaras G G 2008 Enzymatic sensing with organic electrochemical transistors *J. Mater. Chem.* **18** 116–20

[55] Yaghmazadeh O, Cicoira F, Bernards D A, Yang S Y, Bonnassieux Y and Malliaras G G 2011 Optimization of organic electrochemical transistors for sensor applications *J. Polym. Sci.* B **49** 34–9

[56] Tanase C, Meijer E J, Blom P W M and de Leeuw D M 2003 Unification of the hole transport in polymeric field-effect transistors and light-emitting diodes *Phys. Rev. Lett.* **91** 216601

[57] Campbell A J, Rawcliffe R, Guite A, Faria J C D, Mukherjee A, McLachlan M A, Shkunov M and Bradley D D C 2016 Charge-carrier density independent mobility in amorphous fluorene-triarylamine copolymers *Adv. Funct. Mater.* **26** 3720–9

[58] Garcia-Belmonte G, Munar A, Barea E M, Bisquert J, Ugarte I and Pacios R 2008 Charge carrier mobility and lifetime of organic bulk heterojunctions analyzed by impedance spectroscopy *Org. Electron.* **9** 847–51

[59] Lago N *et al* 2016 A physical-based equivalent circuit model for an organic/electrolyte interface *Org. Electron.* **35** 176–85

[60] Decarlo R A and Min P-M 1995 *Linear Circuit Analysis: Time Domain, Phasor, and Laplace Transform Approaches* 2nd Edition (Oxford: Oxford University Press)

[61] Khodagholy D *et al* 2013 High transconductance organic electrochemical transistors *Nat. Commun.* **4** 2133

[62] Tria S A, Jimison L H, Hama A, Bongo M and Owens R M 2013 Validation of the organic electrochemical transistor for *in vitro* toxicology *Biochim. Biophys. Acta* **1830** 4381–90

[63] Rivnay J, Inal S, Collins B A, Sessolo M, Stavrinidou E, Strakosas X, Tassone C, Delongchamp D M and Malliaras G G 2016 Structural control of mixed ionic and electronic transport in conducting polymers *Nat. Commun.* **7** 11287

[64] Musumeci C, Vagin M, Zeglio E, Ouyang L, Gabrielsson R and Inganäs O 2019 Organic electrochemical transistors from supramolecular complexes of conjugated polyelectrolyte PEDOTS *J. Mater. Chem.* C **7** 2987–93

[65] Shoar Abouzari M R, Berkemeier F, Schmitz G and Wilmer D 2009 On the physical interpretation of constant phase elements *Solid State Ionics* **180** 922–7

[66] Taylor S R and Gileadi E 1995 Physical interpretation of the Warburg impedance *Corrosion* **51** 664–71